[10] M. Jiang *et al*., "Solving scattering by multilayer dielectric objects using JMCFIE-DDM-MLFMA," *IEEE Antennas Wireless Propag. Lett*., vol. 13, pp. 1132–1135, Jun. 2014.
[11] L. Matekovits, V. A. Laza, and G. Vecchi, "Analysis of large complex structures with the synthetic-functions approach," *IEEE Trans. Antennas Propag*., vol. 55. no. 9, pp. 2509–2521, Sep. 2007.
[12] A. Freni, P. D. Vita, P. Pirinoli, L. Matekovits, and G. Vecchi, "Fast-factorization acceleration of MoM compressive domain-decomposition," *IEEE Trans. Antennas Propag*., vol. 59, no. 12, pp. 4588–4599, Dec. 2011.
[13] O. Wiedenmann and T. F. Eibert, "A domain decomposition method for boundary integral equations using a transmission condition based on the near-zone couplings," *IEEE Trans. Antennas Propag*., vol. 62, no. 8, pp. 4105–4114, Aug. 2014.
[14] X. Wang, Z. Peng, and J.-F. Lee, "A new integral equation based domain decomposition method for electromagnetic analysis of large multi-scale problems," in *Proc. IEEE Antennas Propag. Soc. Int. Symp*., 2012, pp. 1–2.
[15] X. Wang, "A domain decomposition method for analysis of three-dimensional large-scale electromagnetic compatibility problems," Ph.D. dissertation, Ohio State Univ., Columbus, OH, USA, 2012.
[16] S. M. Rao, D. Wilton, and A. W. Glisson, "Electromagnetic scattering by surfaces of arbitrary shape," *IEEE Trans. Antennas Propag*., vol. 30, no. 3, pp. 409–418, May 1982.
[17] P. Ylä-Oijala and M. Taskinen, "Calculation of CFIE impedance matrix elements with RWG and $n \times$ RWG functions," *IEEE Trans. Antennas Propag*., vol. 51, no. 8, pp. 1837–1846, Aug. 2003.
[18] R. Barrett *et al*., *Templates for the Solution of Linear Systems: Building Blocks for Iterative Methods*. Philadelphia, PA, USA: SIAM, 1994 [Online]. Available: http://www.netlib.org/templates/templates.pdf
[19] C. T. Kelley, *Iterative Methods for Linear and Nonlinear Equations*. Philadelphia, PA, USA: SIAM, 1995.
[20] A. C. Woo, H. T. G. Wang, and M. J. Schuh, "Benchmark radar targets for the validation of computational electromagnetics programs," *IEEE Antennas Propag. Mag*., vol. 35, no. 1, pp. 84–89, Feb. 1993.

A Compact and Low-Profile Loop Antenna With Multiband Operation for Ultra-Thin Smartphones

Di Wu, S. W. Cheung, and T. I. Yuk

***Abstract*—A folded loop antenna having a very compact size of $5 \times 8 \times 60\ \mathrm{mm}^3$ with multiband operation for ultra-thin smartphone applications is proposed. The antenna generates four resonant modes, the traditional 0.5-λ, 1-λ, and 1.5-λ resonant modes and an extra higher-order 2-λ resonant mode, to cover the GSM850, GSM900, DCS1800, PCS1900, UMTS, TD-SCDMA, LTE2300, and WLAN systems. The extra 2-λ resonant mode is generated using a certain distance between the feed point and the shorting point on the ground plane. The antenna is studied using simulation and measurement. To study the antenna in a more realistic situation, a standard metallic USB connector is placed inside the loop radiator. Results show that the USB connector has little effects on the antenna performance.**

***Index Terms*—Loop antenna, mobile antennas, multiband antenna, multimode antenna.**

I. Introduction

With the increasing popularity of ultra-thin smartphones such as the iPhones and Samsung Notes, etc., antennas designers are facing the challenge of designing compact and low-profile antennas with multiband operations [1], [2]. The common types of mobile antenna for wideband operations are monopole antennas [3], [4], inverted-F antennas (IFAs) [5], [6], and frequency reconfigurable antennas [7], [8]. There are also other innovative techniques such making use the metallic rim of the smartphone [9] and using nonresonant planar elements [10].

Loop antenna, with the feature of multiresonant mode, is a potential candidate for the design of compact and low-profile antennas for small mobile phones requiring multiband operations and so is attracting attention [11]–[14]. However, all the loop antennas studied in [11]–[14] could generate only three resonant modes, the 0.5-λ, 1-λ, and 1.5-λ modes [11]–[14], which limited their operating bandwidths. In these designs, the 0.5-λ mode was used to generate a low-frequency band, and the 1-λ and 1.5-λ modes together were used to generate a high-frequency band. Recently, a three-dimensional (3-D) loop antenna having a higher resonant mode, the 2-λ mode, was reported in [15]. The authors did not give explanation on how the 2-λ mode was generated.

In this communication, a 3-D loop antenna, having four resonant modes, the 0.5-λ, 1-λ, 1.5-λ, and 2-λ modes, used to generate two wide frequency bands, is presented and studied. The low-frequency band has a bandwidth of 0.8–1.1 GHz (0.3 GHz or 15.7%) to cover the GSM850 and GSM900 systems, while the higher frequency band has a bandwidth of 1.7–2.58 GHz (0.88 GHz or 40%) to cover the DCS1800, PCS1900, UMTS, TD-SCDMA, LTE2300, and 2.4-GHz WiFi systems. The loop radiator consists of a folded loop strip and two tuning arms, with a very compact volume of only $5 \times 8 \times 60\,\mathrm{mm}^3$. By adjusting the distance between the feed point and the shorting point of

Manuscript received December 06, 2014; revised February 12, 2015; accepted March 02, 2015. Date of publication March 16, 2015; date of current version May 29, 2015.

The authors are with the Department of Electrical and Electronic Engineering, The University of Hong Kong, Hong Kong (e-mail: diwu@eee.hku.hk; swcheung@eee.hku.hk; tiyuk@eee.hku.hk).

Color versions of one or more of the figures in this communication are available online at http://ieeexplore.ieee.org.

Digital Object Identifier 10.1109/TAP.2015.2412962

the loop radiator, a higher-order resonant mode (i.e., the 2-λ mode) is generated, which combines with the 1-λ and the 1.5-λ modes to generate a high-frequency band with a very wide bandwidth. The effects of having a standard metallic USB connector on the antenna performance are also studied in this communication. In order to not to increase the thickness of the mobile phone, the metallic USB connector is placed inside the loop radiator. Results show that the USB connector only has little effects on the antenna performance. The antenna is studied using the EM simulation tool CST. For verification, the antenna is also fabricated and measured using the antenna measurement equipment, the Satimo Starlab system.

II. Antenna Design

The geometry of the proposed 3-D loop antenna for mobile phone applications is shown in Fig. 1. It is designed on a single-sided PCB with an area of $120 \times 60\,\mathrm{mm}^2$, as shown in Fig. 1(a). A clearance area of $8 \times 60\,\mathrm{mm}^2$ at the bottom edge of the PCB is made available to accommodate the antenna. The rest of the PCB, with an area of $112 \times 60\,\mathrm{mm}^2$, serves as system ground. Putting the antenna near to the bottom edge of the phone allows other metallic electronic blocks such as the receiver, camera, proximity sensor, and power switch, etc., to be placed on the upper region of the PCB so as to reduce their effects on the antenna performance. This can also reduce the effects of human head and hand on the antenna, and the measured value of specific absorption rate (SAR).

The loop strip (radiator) of the loop antenna, as shown in Fig. 1, has one end connected to the feed point and another end connected to the ground plane via a shorting pin. The total loop length, from the feed point to the shorting point, is about 210 mm (equivalent to 0.5λ at 800 MHz) to generate the 0.5-λ, 1-λ, and 1.5-λ modes at about 0.8, 1.78, and 2.04 GHz, respectively [13]. By adjusting the distance between the feed point and the shorting point on the ground plane, a higher-order resonant mode, the 2-λ mode, at about 2.46 GHz can be generated, as will be shown later. In the present design, the 0.5-λ mode generates a low-frequency band with quite a narrow bandwidth, while the 1-λ, 1.5-λ, and 2-λ modes together generate a wide high-frequency band. A high-pass filter, composed of a series chip capacitance $\mathrm{C} = 3.3\,\mathrm{pF}$ (Murata 0402) and a shunt chip inductance $\mathrm{L} = 12\,\mathrm{nH}$ (Murata 0402), as shown in Fig. 1(b), is employed as a matching circuit to enhance the bandwidth of the low-frequency band without affecting the high-frequency band. The frequencies in the 1.5-λ and 2-λ modes can be tuned using the two tuning arms, tuning arms 1 and 2, respectively, in the radiator as shown in Fig. 1(a) (which was proposed in [13]). To reduce the volume, the radiator is meandered and folded, as shown in Fig. 1. In Fig. 1(c), the dashed lines are for folding the radiator. After folding, points A & A^1 and points B & B^1 indicated in Fig. 1(c) are joined together. The loop antenna is studied and designed using the EM simulation tool CST on a substrate with a thickness of 0.8 mm, a relative permittivity of 3.5 and a loss tangent of 0.02. The final dimensions of the antenna are shown in Table I and used to fabricate the prototyped antenna as shown in Fig. 2 for measurement. In the prototyped antenna, the loop radiator is fixed on a rectangular-shaped foam with the permittivity close to that of air ($\varepsilon_r = 1.0$). The loop radiator has a height of 5 mm and is surface mounted on a clearance area of $8 \times 60\,\mathrm{mm}^2$ on the PCB as shown in Fig. 2. Thus the loop radiator has a total volume of only $60 \times 8 \times 5\,\mathrm{mm}^3$, which is very compact and low profile and is suitable for uses in the current ultra-thin smartphones.

The distance between the feed point and shorting point is quite critical in generating and setting the 2-λ mode, which is optimized to be 20 mm using computer simulation. The space inside the loop radiator should not be wasted, so we propose to use it to accommodate a standard USB connector which will be studied later in this communication.

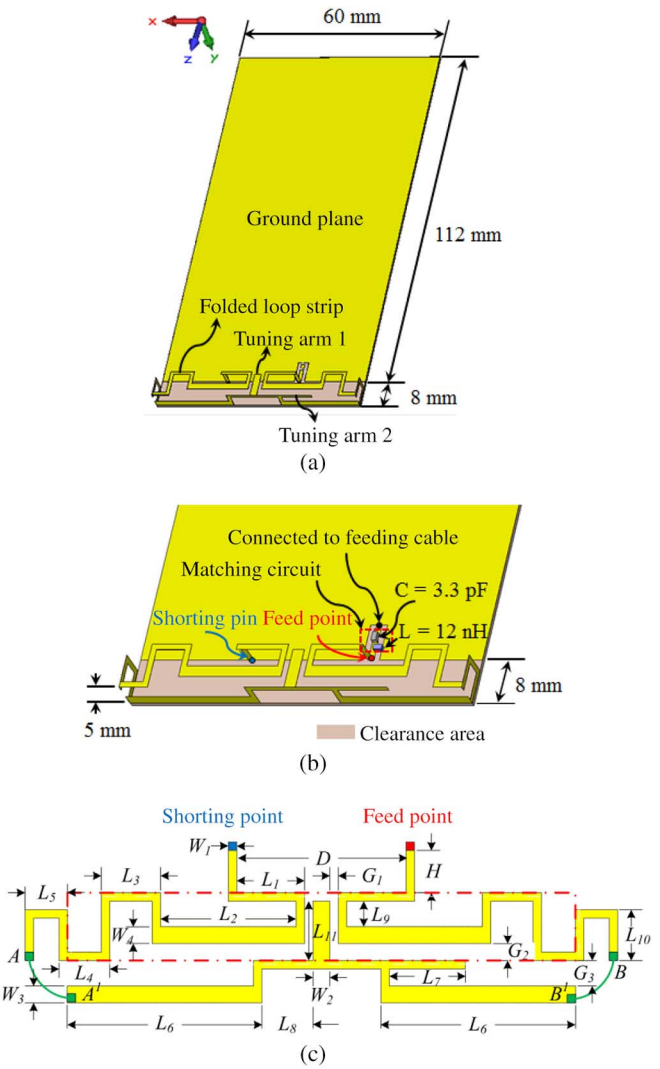

Fig. 1. Geometry and dimensions of proposed antenna: (a) 3-D view with ground plane; (b) enlarged 3-D view with matching circuit; and (c) 2-D view of loop radiator (_._. folded line).

TABLE I
Dimensions of Proposed Antenna (mm)

L_1	L_2	L_3	L_4	L_5	L_6	L_7	L_8	L_9	L_{10}
8	16	7	6	5	23	9	6	3	6
L_{11}	W_1	W_2	W_3	W_4	G_1	G_2	G_3	H	D
7	1	2	2	2	1	2	3	5	20

III. Parameter Study

As mentioned previously, the distance D between the feed point and the shorting point of the loop antenna is used to generate the 2-λ mode. To illustrate how the 2-λ mode is generated, the simulated S_{11} with $D = 1$, 4, 12, 20, and 28 mm are shown in Fig. 3. Note that when $D = 1$ mm, the space between the feed point and shorting point as shown in Fig. 1 is too small to accommodate tuning arm 2

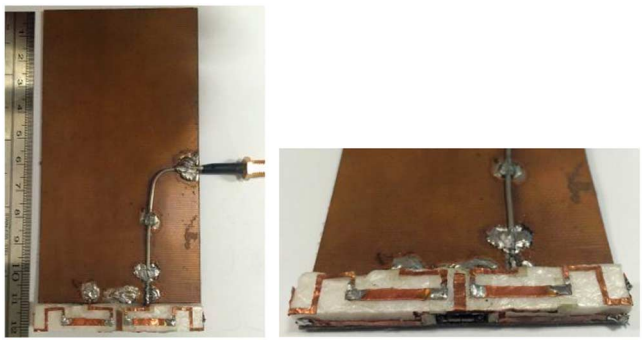

Fig. 2. Prototyped antenna.

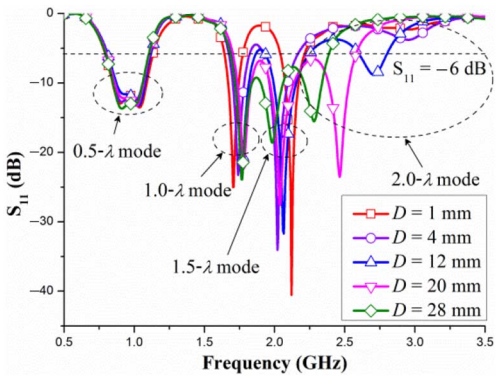

Fig. 3. Simulated S_{11} of proposed antenna with different values of D.

which therefore is removed in the model. It can be seen in Fig. 3 that, with $D = 1$ mm, the resonance in the 2-λ mode is quite weak ($S_{11} = -2$ dB) and cannot form a frequency band. As D increases from 1 to 4, 12, 20, and then 28 mm, the resonance in the 2-λ mode becomes stronger ($S_{11} < -6$ dB) and shifts to lower frequencies from 2.96 to 2.95, 2.71, 2.46, and 2.28 GHz, respectively. The resonant frequencies in the other resonant modes (the 0.5-λ, 1-λ, and 1.5-λ modes) change only slightly. This result indicates that the 2-λ mode can be generated using a large D and independently tuned without affecting the other resonances. The distance D has been optimized in terms of maximizing the bandwidth using simulation to be 20 mm. Fig. 3 shows that the 2-λ mode combined with the 1-λ and 1.5-λ modes forms a wide high-frequency band of 1.7–2.58 GHz which can accommodate the DCS1800, PCS1900, UMTS2100, TD-SCDMA, LTE2300, and 2.4G-WiFi systems.

The operation of the loop antenna is further studied using vector-surface current distribution and results are shown in Fig. 4. Note that these figures are two-dimensional (2-D) views of the radiator facing the negative y-axis direction in Fig. 1. At 0.9, 1.78, 2.04, and 2.46 GHz, the center frequencies of the four resonances, Fig. 4(a)–(d) show that there are one, two, three, and four current nulls (represented as $\otimes$ on the figures), respectively, on the loop strip, indicating that the antenna is operating in the 0.5-λ, 1-λ, 1.5-λ, and 2-λ modes, respectively. Fig. 4(a) and (c) shows that the currents at the feed point and shorting pin have the same direction and the currents along the lower edge of the ground plane have the opposite directions. These indicate that the antenna in the 0.5-λ and 1.5-λ modes is operating in a common mode. Fig. 4(b) and (d) shows that the currents at the feed point and shorting pin have the opposite directions, which indicate that the antenna in the 1-λ and 2-λ modes is operating in a differential mode [16]. In Fig. 4(b), the currents along the lower edge of the ground plane mainly have the same direction to the right. In Fig. 4(d),

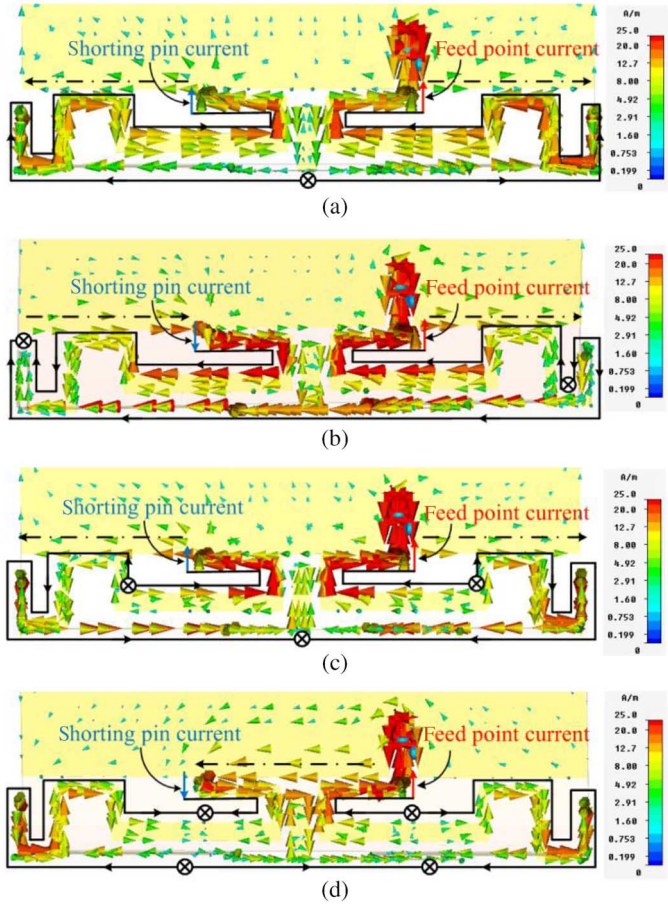

Fig. 4. Simulated vector-current distributions of loop antenna at frequencies of: (a) 0.9 GHz; (b) 1.78 GHz; (c) 2.04 GHz; and (d) 2.46 GHz (_._.current on ground plane; $\otimes$ current null).

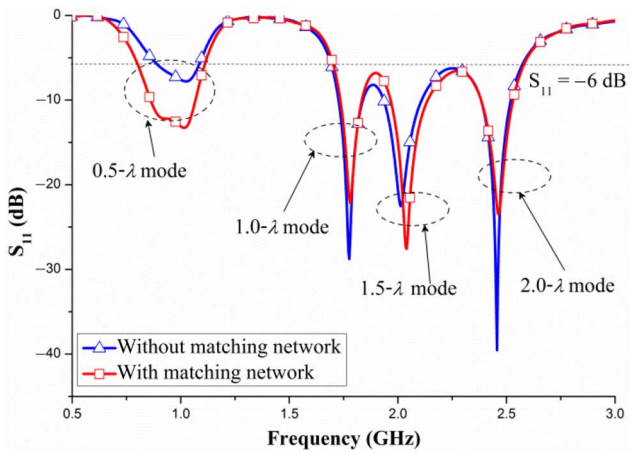

Fig. 5. Simulated S_{11} of proposed antenna with and without matching circuit.

the currents along the lower edge of the ground plane mainly flow from the feed point to the shorting point.

The simulated S_{11} of the antenna with and without the matching circuit are shown in Fig. 5. With the matching circuit, the bandwidth (for $S_{11} < -6$ dB or VSWR $= 3:1$) of the low-frequency band is increased from 0.9–1.08 GHz (180 MHz or 18%) to 0.8–1.10 GHz (303 MHz or 32%), while the bandwidth of the high-frequency band remains unchanged from 1.7 to 2.58 GHz (0.88 GHz or 41%).

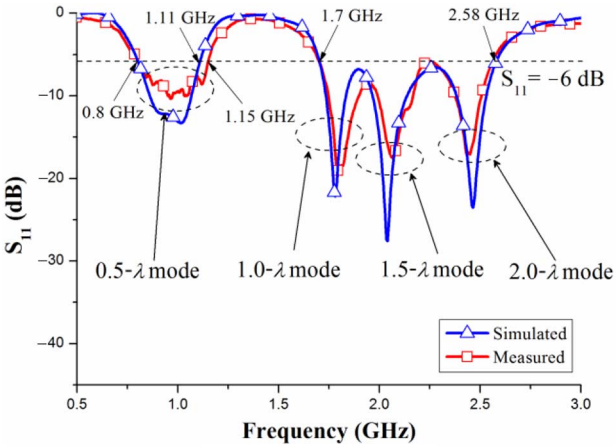

Fig. 6. Simulated and measured S_{11} of loop antenna.

IV. Simulation and Measurement Results

The loop antenna of Fig. 1 has been simulated and the prototyped antenna of Fig. 2 has been measured. The simulated and measured S_{11} are shown in Fig. 6 which indicates a good agreement. Although the vector-current distributions at 1.78 and 2.46 GHz shown in Fig. 4(b) and (d) indicate that the antenna is operating in the 1-λ and 2-λ modes, respectively, due to the capacitive and inductive effects between the branches and on the branches of the loop radiator, the frequency in the 2-λ mode is not twice as that in the 1-λ mode. It can be seen in Fig. 6 that the 0.5-λ resonant mode forms a low-frequency band with a bandwidth ($S_{11} < -6$ dB) of 0.8–1.1 GHz (0.35 GHz, 35.9%), and the 1-λ, 1.5-λ, and 2-λ modes together form a high-frequency band with a bandwidth of 1.7–2.58 GHz (0.86 GHz, 40.4%). Thus the proposed loop antenna can support the 2G, 3G, 4G, and LTE systems such as the GSM (including GSM850, GSM900, DCS1800, and PCS1900), UMTS, TD-SCDMA (Band A/F), LTE 2300, and 2.4-GHz WiFi systems.

The antenna measurement equipment, Satimo StarLab System [17], is used to measure the efficiency of the antenna. The equipment first measures the gain, radiation intensity, and reflection coefficient and then computes the directivity using the radiation intensity [18]. Finally, it computes the efficiency using

$$\textit{Efficiency} = \frac{G(\theta,\varphi)}{D(\theta,\varphi)}(1-|\Gamma|^2) \tag{1}$$

where Γ is the voltage reflection coefficient, $G(\theta,\phi)$ and $D(\theta,\phi)$ are the gain and directivity, respectively, of the antenna and are functions of spherical coordinate angles θ and ϕ. The simulated and measured efficiencies of the antenna are shown in Fig. 7(a), which again shows a good agreement. The discrepancy is mainly due to the measurement and fabrication tolerances, cable effects used in measurement [19], and also the ohmic loss of the lumped matching circuit [the series chip capacitor C and shunt chip inductor L in Fig. 1(b)] not being considered in simulation. Fig. 7(a) shows that the measured efficiency (including the mismatching loss) ranges from 50% to 76% in the lower band (0.8–1.1 GHz) and 57% to 84% in the higher band (1.71–2.58 GHz), which are acceptable for practical mobile antennas [20]–[22]. Fig. 7(b) shows that the measured realized peak gain is about 0.96–2.4 dBi in the lower band and 3.2–4.5 dBi in the higher band.

The simulated and measured 3-D radiation patterns at the resonant frequencies of 0.9, 1.78, 2.04, and 2.46 GHz are shown in Fig. 8. The simulated and measured results show good agreement. At 0.9 GHz in the lower band, Fig. 8(a) shows that the antenna has a dipole-like radiation pattern in the *y*–*z* plane and an omnidirectional radiation pattern in the *x*–*y* plane. At 1.78 GHz, the antenna does not behave like a dipole, but has relatively omnidirectional radiation patterns in the *x*–*y* and *y*–*z* planes as shown in Fig. 8(b). At 2.04 GHz, Fig. 8(c) shows that the radiation pattern has a double-donut shape with much stronger radiation in the upper hemisphere. Thus, in the two common modes at 0.9 and 2.04 GHz, the radiation patterns are similar to those of traditional mobile antennas such as PIFA and monopole [1], [5]. For in two differential modes at 1.78 and 2.46 GHz, the radiation patterns are relatively omnidirectional, which are also useful for mobile phone applications.

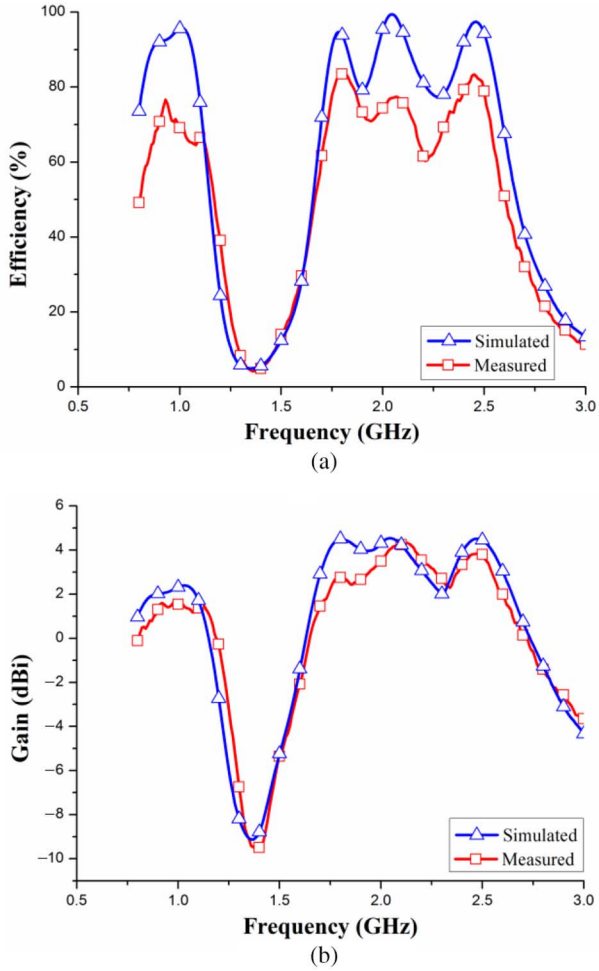

Fig. 7. Simulated and measured (a) efficiencies and (b) gains of loop antenna.

V. Effects of Nearby Metallic USB Connector

As mentioned previously, to make the smartphone thinner, we propose to put the metallic USB connector inside the loop radiator as shown in the simulation model of Fig. 9. The metallic USB has a standard volume of $L_u \times W_u \times H_u$ mm^3 and is mounted on a protruded ground with a size of $L_u \times W_c$ mm^2 as shown in Fig. 9(b). The dimensions of the metallic USB connector and the protruded ground are shown in Table II. There is a gap [with $g_2 = 2$ mm and $g_1 = 1$ mm in Fig. 9(a)] between the USB connector and the antenna radiator. Such a small gap would not be possibly used in traditional mobile antennas such as PIFA, IFA, or monopole because the EM wave from the radiator in the near field would easily coupling into the metallic USB connector and degrade the antenna performance. The loop antenna

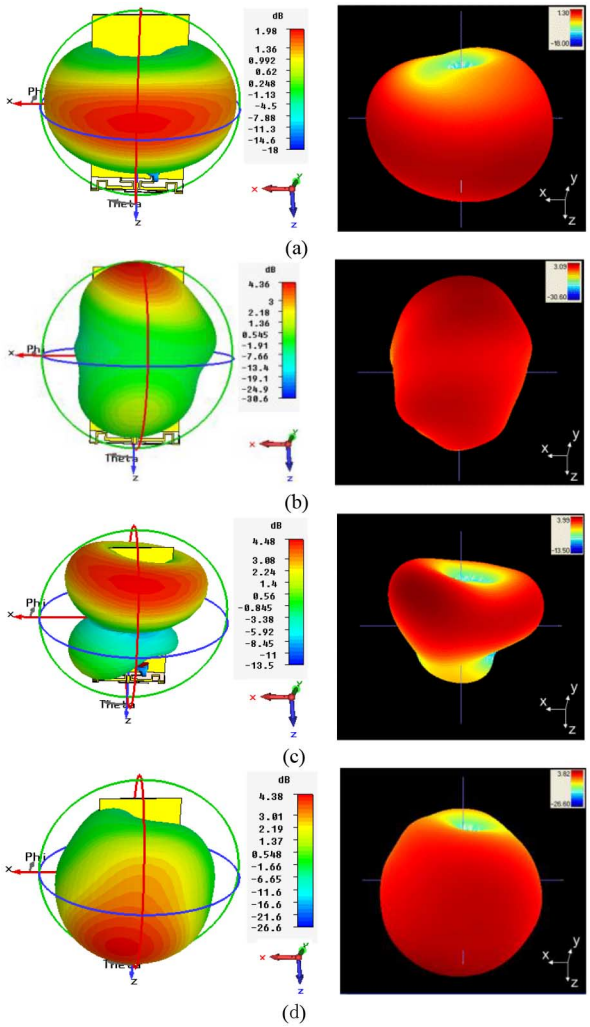

Fig. 8. Simulated (left) and measured (right) radiation patterns at: (a) 0.9 GHz; (b) 1.78 GHz; (c) 2.04 GHz; and (d) 2.46 GHz.

with a real metallic USB connector is studied using simulation and fabricated as shown in Fig. 2 for measurement.

The simulated and measured S_{11} of the antenna with and without having the USB connector are shown in Fig. 10. The simulated and measured results show good agreement. The USB connector has little effects on the resonant frequencies of the antenna. With the USB connector, the simulated resonant frequency in the 0.5-λ mode slightly shifts down, resulting in a bandwidth of 0.77–1.02 GHz for the lower band, which still can cover the frequency bands for GSM850 and GSM900 systems. The measured bandwidth in the lower band is about 0.77–1.08 GHz. The simulated and measured bandwidths in the higher band remain the same of about 1.7–2.58 GHz.

The simulated and measured efficiencies with and without the USB connector are shown in Fig. 11 which shows good agreement. The discrepancies are due to the factors mentioned previously and also the accuracy of the simulation model for the USB connector. Fig. 11 shows that the USB connector slightly increases the efficiency in the lower band. The range of measured efficiency in the lower band of 0.8–1.1 GHz increases from about 50%–76% to about 50%–85%. In the higher band of 1.71–2.58 GHz, the range of measured efficiency remains about the same, i.e., 58%–84%.

The reasons why the USB connector inside the loop radiator have little effects on the antenna performance can be explained as follows.

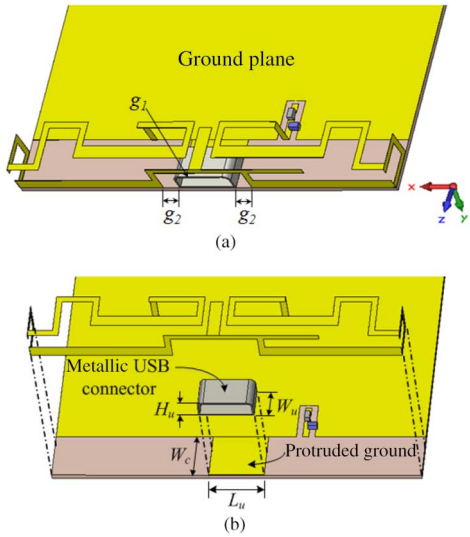

Fig. 9. Simulation model of loop antenna with USB connector: (a) total view and (b) expanded view.

TABLE II
DIMENSIONS OF PLACING USB CONNECTOR (MM)

g_1	g_2	L_u	W_u	H_u	W_c
1	2.5	9	5	3	8

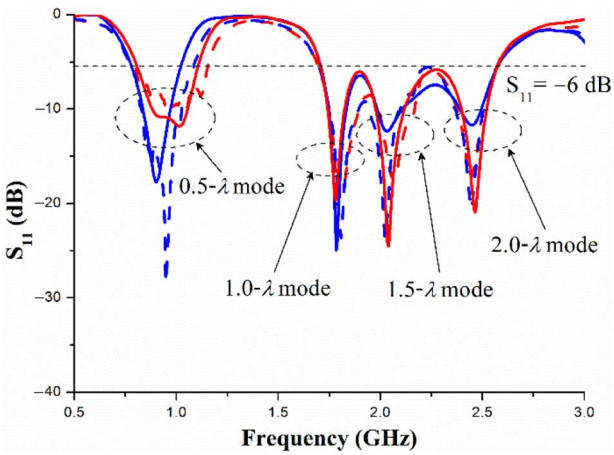

Fig. 10. Simulated and measured S_{11} of loop antenna with and without USB connector (*blue dashed lines:* simulated S_{11} with USB connector; *red dashed lines:* simulated S_{11} without USB connector; *blue dotted line:* measured S_{11} with USB connector; *red dotted line:* measured S_{11} without USB connector).

In the two common modes of 0.5-λ and 1.5-λ, Fig. 4(a) and (c) shows that the current paths have a null near the USB connector and the currents on the portion of radiator above the USB connector are quite weak. In the two differential modes of 1-λ and 2-λ, Fig. 4(b) and (d) shows that the currents on the radiator region above the USB connector are quite weak and in opposite directions, so that their effects cancel off. Since the currents close to the USB connector are very weak, the USB connector has little effects on the antenna performance.

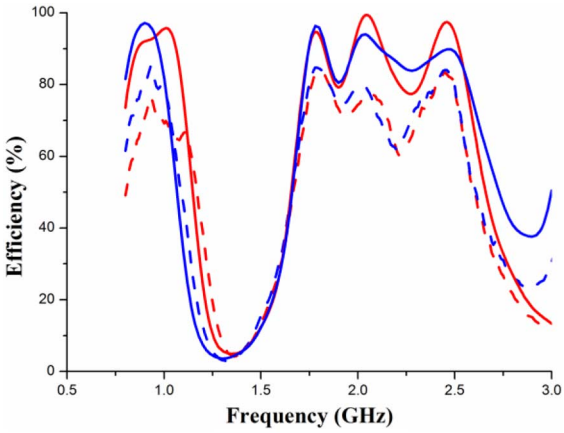

Fig. 11. Simulated and measured efficiency of loop antenna with and without USB connector (*blue dashed lines:* simulated efficiency with USB connector; *red dashed lines:* simulated efficiency without USB connector; *blue dotted line:* measured efficiency with USB connector; *red dotted line:* measured efficiency without USB connector).

VI. Conclusion

A folded loop antenna having four resonant modes for use in ultra-thin smartphones has been proposed and studied. The loop radiator of the antenna consists of a loop strip and two tuning arms, with a very compact volume of only $5 \times 8 \times 60\,\text{mm}^3$. The four resonant modes generated include the three commonly known resonant modes of 0.5-λ, 1-λ, and 1.5-λ, and an additional mode of 2-λ. The 0.5-λ is used to generate a lower band, while the 1-λ, 1.5-λ, and 2-λ together are used to generate a higher band. Simulated and measured results have shown that the loop antenna can provide two wide operating bands, 0.8–1.1 GHz and 1.7–2.58 GHz, to cover most of the frequency bands for the 2G, 3G, 4G-LTE, and 2.4-GHz WiFi systems. The effects of a standard metallic USB connector placed inside the loop radiator have also been studied using simulation and measurement. Results have shown that the USB connector has little effects on the antenna performance. All these results indicate that the proposed loop antenna is a very promising candidate for the design of practical ultra-slim smartphones.

References

[1] K. L. Wong, *Planar Antennas for Wireless Communications*. Hoboken, NJ, USA: Wiley Inter-Science, 2003.

[2] J. Anguera *et al*., "Advances in antenna technology for wireless handheld devices," *Int. J. Antennas Propag*., vol. 2013, 25 p., 2013, Article ID 8383643 [Online]. Available: http://dx.doi.org/10.1155/2013/838364

[3] K. L. Wong and S. C. Chen, "Printed single-strip monopole using a chip inductor for penta-band WWAN operation in the mobile phone," *IEEE Trans. Antennas Propag*., vol. 58, no. 3, pp. 1011–1014, Mar. 2010.

[4] Y. L. Ban, Y. F. Qiang, Z. Chen, K. Kang, and J. Li, "Low-profile narrow-frame antenna for seven-band WWAN/LTE smartphone applications," *IEEE Antennas Wireless Propag. Lett*., vol. 13, pp. 463–466, Mar. 2014.

[5] Z. J. Zhang, *Antenna Design for Mobile Devices*. Hoboken, NJ, USA: Wiley, 2011.

[6] C. H. Wu and K. L. Wong, "Ultrawideband PIFA with a capacitive feed for penta-band folder-type mobile phone antenna," *IEEE Trans. Antennas Propag*., vol. 57, no. 8, pp. 2461–2464, Aug. 2009.

[7] Y. Li, Z. J. Zhang, J. F. Zheng, Z. H. Feng, and M. F. Iskander, "A compact hepta-band loop-inverted F reconfigurable antenna for mobile phone," *IEEE Trans. Antennas Propag*., vol. 60, no. 1, pp. 389–392, Jan. 2012.

[8] Y. Li, Z. J. Zhang, J. F. Zheng, and Z. H. Feng, "Compact heptaband reconfigurable loop antenna for mobile handset," *IEEE Antenna Wireless Propag. Lett*., vol. 10, pp. 1162–1165, Oct. 2011.

[9] Y. L. Ban, Y. F. Qiang, Z. Chen, K. Kang, and J. H. Guo, "A dual-loop antenna design for hepta-band WWAN/LTE metal-rimmed smartphone application," *IEEE Trans. Antennas Propag*., vol. 63, no, 1, pp. 48–58, Jan. 2015.

[10] J. Anguera, A. Andújar, and C. García, "Multiband and small coplanar antenna system for wireless handheld devices," *IEEE Trans. Antennas Propag*., vol. 61, no. 7, pp. 3782–3789, Jul. 2013.

[11] Y. W. Chi and K. L. Wong, "Internal compact dual-band printed loop antenna for mobile phone application," *IEEE Trans. Antennas Propag*., vol. 55, no. 5, pp. 1457–1462, May 2007.

[12] K. L. Wong and C. H. Huang, "Printed loop antenna with a perpendicular feed for penta-band mobile phone application," *IEEE Trans. Antennas Propag*., vol. 56, no. 7, pp. 2138–2141, Jul. 2008.

[13] Y. W. Chi and K. L. Wong, "Compact multiband folded loop chip antenna for small-size mobile phone," *IEEE Trans. Antennas Propag*., vol. 56, no. 12, pp. 3797–3803, Dec. 2008.

[14] K. Ishimiya, C. Y. Chiu, and J. Takada, "Multiband loop handset antenna with less ground clearance," *IEEE Antennas Wireless Propag. Lett*., vol. 12, pp. 1444–1447, Nov. 2013.

[15] M. Zheng, H. Y. Wang, and Y. Hao, "Internal hexa-band folded monopole/dipole/loop antenna with four resonances for mobile device," *IEEE Trans. Antennas Propag*., vol. 60, no. 6, pp. 2880–2885, Jun. 2012.

[16] K. R. Boyle and L. P. Ligthart, "Radiating and balanced mode analysis of PIFA antennas," *IEEE Trans. Antennas Propag*., vol. 54, no. 1, pp. 231–237, Jan. 2006.

[17] [Online]. Available: http://www.satimo.com/

[18] C. A. Balanis, *Antenna Theory–Analysis and Design*, 3rd ed. Hoboken, NJ, USA: Wiley, 2005.

[19] L. Liu, Y. F. Weng, S. W. Cheung, T. I. Yuk, and L. J. Foged, "Modeling of cable for measurements of small monopole antennas," presented at the Loughborough Antennas Propag. Conf. (LAPC 2011), Loughborough, U.K., Nov. 14–15, 2011.

[20] K. L. Wong and T. W. Weng, "Small-size triple-wideband LTE/WWAN tablet device antenna," *IEEE Antennas Wireless Propag. Lett*., vol. 12, pp. 1516–1519, Nov. 2013.

[21] Y. L. Ban, J. H. Chen, S. Yang, J. Li, and Y. J. Wu, "Low-profile printed octa-band LTE/WWAN mobile phone antenna using embedded parallel resonant structure," *IEEE Trans. Antennas Propag*., vol. 61, no. 7, pp. 3889–3894, Jul. 2013.

[22] K. L. Wong and L. Y. Chen, "Small-size LTE/WWAN tablet device antenna with two hybrid feeds," *IEEE Trans. Antennas Propag*., vol. 60, no. 6, pp. 2926–2934, Jun. 2014.